PERFORMANCE EVALUATION AND TEST RESULTS OF A 11,000r/min, 4kW SURFACE-MOUNTED PERMANENT MAGNET-TYPE BEARINGLESS MOTOR

Masahide Ooshima, Satoru Miyazawa
Department of Electronics Engineering, Science University of Tokyo Suwa College
Chino, Nagano, Japan, moshima@sd.suwa.sut.ac.jp
Akira Chiba, Fukuzo Nakamura
Department of Electrical Engineering, Faculty of Science and Technology,
Science University of Tokyo, Noda, Chiba, Japan, chiba@ee.noda.sut.ac.jp
Tadashi Fukao
Department of Electrical and Electronic Engineering, Faculty of Technology,
Tokyo Institute of Technology, Meguro, Tokyo, Japan, tfukao@ee.titech.ac.jp

ABSTRACT
Recently, bearingless motors are actively developed and researched. The rotor suspension control algorithms have been already proposed and tested by prototype machines. To apply the bearingless motors in industry fields, it is necessary that the performance evaluations as electric motors as well as the rotor suspension characteristics are found. In this paper, a prototype 11,000r/min, 4kW surface-mounted permanent magnet-type bearingless motor is constructed. The rotor radial position control method, in which an influence of armature reaction to the bearingless motor magnetic field is considered, is presented. Then, it is confirmed that the rotor shaft is successfully suspended by electromagnetic forces even in a high speed operation. In addition, the motor characteristics of the rotational torque, the efficiency, etc. as well as the necessary power for the rotor suspension are measured by the load tests. The performance of the prototype machine as an electric motor is evaluated by the measured motor characteristics.

INTRODUCTION
Bearingless motors have attracted attentions in high speed electric motors and motors operated under special circumstances, for example, in vacuum and under high temperature. The bearingless motors are actively developed and researched to apply to machine tools, liquid pumps, compressors, etc. The bearingless motors are hybrids of electric motors and magnetic bearings. Therefore, high speed operation, miniaturization of overall equipment size and low cost can be realized.
In the bearingless motor structures, radial force windings as well as motor windings are additionally wound in the stator iron core. A rotational torque is generated by the motor winding currents, and the principle is the same as that of conventional electric motors. The currents in the radial force windings result in the radial force flux, therefore, radial force flux as well as the motor flux for the rotational torque generation exists in the bearingless motor field. The airgap flux densities are properly unbalanced by the radial force flux. As a result, the rotor shaft is successfully suspended by the electromagnetic forces. The principle of the bearingless motors can be applied to several kinds of conventional motor types. The principles, the structures, the rotor position control strategies and the rotor suspension test results have been already made clear[1]-[8].
In the permanent magnet-type bearingless motors, armature reaction is generated, and both a magnitude and a direction of airgap flux are dependent on the motor load. Therefore, it is necessary that information on both the magnitude and the direction of airgap flux is accurately obtained to control the rotor radial position. If an airgap length is large and a permanent magnet thickness is thick in a bearingless motor structure, an influence of armature reaction can be neglected in a rotor radial position control[1],[2]. However, the small airgap length and the thin permanent magnet are preferred to generate the radial forces effectively[3]. As a result, armature reaction is easily generated even for the small motor drive current. So, the radial position control method have been already reported considering armature reaction[4],[5]. The rotor position is successfully controlled based on the information on the airgap flux detected by hall sensors.
In most of previously reported papers with respect to the bearingless motors, the rotor suspension control

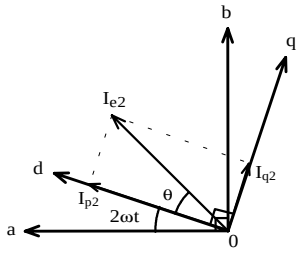

FIGURE 1: Coordinate Transformation

strategies and characteristics have focussed rather than the motor characteristics. However, the performance evaluations as electric motors are also needed to apply the bearingless motors in industry fields. In addition, it is also important that the percentage of the necessary power for the rotor suspension to the power for the motor drive is found.

In this paper, the rotor position control method, in which the magnitude and the direction of the airgap flux are assumed by calculating the field excitation of the permanent magnets and the q-axis flux, is described. Then, a prototype 11,000r/min, 4kW surface-mounted permanent magnet-type bearingless motor, which the rotational speed and the motor capability are enough to apply to general-use liquid pumps, is constructed. It is confirmed that the rotor shaft can be successfully suspended by the electromagnetic forces even in a high speed operation. The motor characteristics of the rotational torque, the efficiency, etc. are shown in the load test results, then, the necessary power for the rotor suspension is also presented. Moreover, the waveforms of the motor and the radial force winding currents as well as the rotor radial displacements are shown.

RADIAL FORCE AND RADIAL FORCE WINDING CURRENT

The relation between the radial force and the radial force winding current is derived in this chapter based on the concept of an equivalent current in the motor winding. The MMF of the permanent magnets is equivalently replaced to that of the motor winding current, then, the equivalent current in the motor winding per phase can be written as

$$\dot{I}_{e2} = I_{p2} + jI_{q2} \quad (1)$$

where $\dot{I}_{e2}$ is denoted by a phasor in two-phase coordinate. I_{p2} is the d-axis component of $\dot{I}_{e2}$. Namely, the field excitation of the permanent magnets can be equivalently represented by a product of I_{p2} and the motor winding inductance. I_{p2} is referred as the equivalent current of the permanent magnets. I_{q2} is the q-axis current. A field weakening control is not done in the control system. Equation (1) can be rewritten as

$$\dot{I}_{e2} = I_{e2}\cos\theta + jI_{e2}\sin\theta \quad (2)$$

where I_{e2} and θ are the amplitude and the phase of the equivalent current $\dot{I}_{e2}$, repectively, and are written as

$$I_{e2} = \sqrt{{I_{p2}}^2 + {I_{q2}}^2} \quad (3)$$

and

$$\theta = tan^{-1}\left(\frac{I_{q2}}{I_{p2}}\right). \quad (4)$$

Transforming $\dot{I}_{e2}$ into currents in a stationary coordinate a- and b-phases as shown in FIGURE 1, the equivalent currents in each phase can be written as

$$i_{ae} = I_{e2}\cos 2(\omega t + \theta/2) \quad (5)$$

$$i_{be} = I_{e2}\sin 2(\omega t + \theta/2) \quad (6)$$

where ω is the mechanical angular speed. 4-pole motors are intended in this paper, therefore, 2ω is the electrical angular speed.

The radial force can be theoretically derived by calculating the magnetic energy stored in the motor and the radial force windings, then, deriving the magnetic energy with respect to the rotor radial displacements[3]. Let us define M' as the derivative of the mutual inductances between the motor and the radial focre windings with respect to the rotor radial displacements. Then, the relations of the radial force components F_α, F_β in two perpendicular axes α, β and the radial force winding currents i_α, i_β in the α- and β-phases can be represented as

$$\begin{bmatrix} i_\alpha \\ i_\beta \end{bmatrix} = \frac{1}{M'I_{e2}} \begin{bmatrix} -\cos 2(\omega t+\theta/2) & \sin 2(\omega t+\theta/2) \\ \sin 2(\omega t+\theta/2) & \cos 2(\omega t+\theta/2) \end{bmatrix} \begin{bmatrix} F_\alpha \\ F_\beta \end{bmatrix}. \quad (7)$$

ROTOR RADIAL POSITION CONTROL SYSTEM

FIGURE 2 shows the system configuration for the surface-mounted permanent magnet-type bearingless motors. The bearingless motor consists of two units. The motor size, the winding distribution and the number of turns of the windings are equal in the units 1 and 2. The motor windings in the units 1 and 2 are connected in series, and the rotational speed is controlled by an inverter. The gap sensors are equipped in two radial axes of each unit. The rotor positioning control in two radial axes is performed in each unit, therefore, the shaft position can be controlled in four radial axes. In the unit 1, the rotor radial displacements α_1 and β_1 to α- and β-directions are detected by the gap sensors, respectively. The errors $\Delta\alpha_1$ and $\Delta\beta_1$ between the detected displacements and the radial position commands α_1^* and β_1^* are amplified by proportional-integral-derivative controllers. Then, the radial force commands $F_{\alpha 1}^*$ and $F_{\beta 1}^*$ are determined. Transforming $F_{\alpha 1}^*$ and $F_{\beta 1}^*$ into the radial force winding current commands $i_{\alpha 1}^*$ and $i_{\beta 1}^*$ in

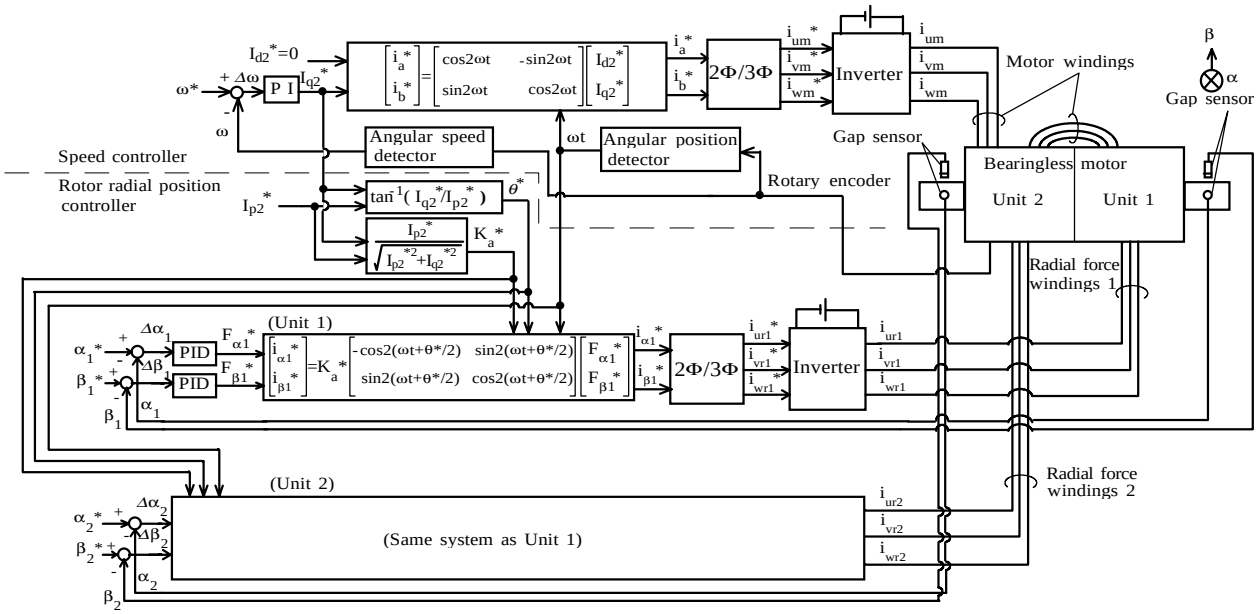

FIGURE 2: System Configuration for Surface-Mounted Permanent Magnet-Type Bearingless Motors

accordance with equation (8), in which equation (7) is referred,

$$\begin{bmatrix} i_{\alpha 1}^{*} \\ i_{\beta 1}^{*} \end{bmatrix} = \frac{1}{M' I_{e2}^{*}} \begin{bmatrix} -\cos 2(\omega t+\theta^{*}/2) & \sin 2(\omega t+\theta^{*}/2) \\ \sin 2(\omega t+\theta^{*}/2) & \cos 2(\omega t+\theta^{*}/2) \end{bmatrix} \begin{bmatrix} F_{\alpha 1}^{*} \\ F_{\beta 1}^{*} \end{bmatrix} \quad (8)$$

where I_{e2}^{*} and θ^{*} can be written as

$$I_{e2}^{*} = \sqrt{I_{p2}^{*2} + I_{q2}^{*2}} \quad (9)$$

and

$$\theta^{*} = \tan^{-1}\left(\frac{I_{q2}^{*}}{I_{p2}^{*}} \right), \quad (10)$$

respectively. I_{p2}^{*} and I_{q2}^{*} are the equivalent current command of the permanent magnets and the q-axis current command, respectively. The error $\Delta\omega$ between the detected rotational angular speed ω and the command ω^{*} is amplified by proportional-integral controller, then, I_{q2}^{*} is determined. I_{p2}^{*} is calculated by the measured motor parameters of the armature reaction reactance, the synchronous internal voltage. In equation (8), the coefficient $1/M'I_{e2}^{*}$ of the radial force commands is rewritten as

$$\frac{1}{M' I_{e2}^{*}} = \frac{1}{M' I_{p2}^{*}} \cdot \frac{I_{p2}^{*}}{\sqrt{I_{p2}^{*2} + I_{q2}^{*2}}} . \quad (11)$$

$1/M'I_{p2}^{*}$ in (11) is constant, and adjusted by the gain in the proportional-integral-derivative controllers. The second term in the right side of (11) is defined as

$$K_a^{*} = \frac{I_{p2}^{*}}{\sqrt{I_{p2}^{*2} + I_{q2}^{*2}}} . \quad (12)$$

K_a^{*} shows the ratio of the field excitation of the permanent magnets to the resultant flux of the field excitation and the q-axis flux. It is well known that a d-axis inductance is equal to a q-axis inductance in machines without saliency. Therefore, the ratio of the fluxes is represented as the calculation with the currents as shown in (12). K_a^{*} is multiplied by $F_{\alpha 1}^{*}$ and $F_{\beta 1}^{*}$. The loop gains in the radial position controller are regulated in accordance with I_{q2}^{*}. The phase command θ^{*} is determined by calculating the ratio of the q-axis flux to the field excitation of the permanent magnets. Similar to K_a^{*}, however, θ^{*} is calculated by the current commands, and regulated by the q-axis current command. Transforming the radial force winding current commands $i_{\alpha 1}^{*}$ and $i_{\beta 1}^{*}$ into the current commands in there-phase coordinate, then, the radial force winding current i_{ur1}, i_{vr1} and i_{wr1} are regulated to follow the current commands. The rotor position control system in the unit 2 is the same as that in the unit 1. K_a^{*} and θ^{*} in the unit 1 are also available in the unit 2 control system. It is possible that the rotor radial positioning is successfully performed by the proposed control strategy without hall sensors. As a result, the simplification of the structure and the decrease in the cost would be realized.

EXPERIMENTAL RESULTS

Experimental Equipment

FIGURE 3 shows the experimental equipment. The dc generator is connected to the bearingless motor as the torque load. The resistor is also connected to the dc generator, and the torque load can be adjusted. The input powers to the motor and the radial force windings

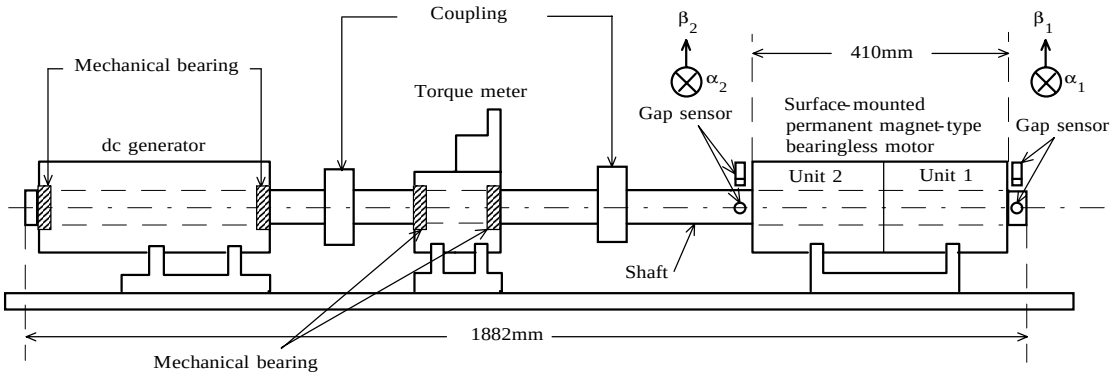

FIGURE 3: Experimental Equipment

TABLE 1: Specification of Prototype Machine

Stator	Outer diameter	133mm
	Inner diameter	73mm
Rotor	Outer diameter	70mm
	Permanent magnets	Sm-Co
	Thickness of permanent magnets	1.5mm
Airgap length		1.5mm
Stack lengths of stator and rotor		45mm (an unit)
Current rating (motor winding)		16A
	(radial force winding)	9.0A
Self-inductance (motor winding)		0.80mH(an unit)
	(radial force winding)	0.70mH(an unit)
Derivative of mutual inductances between motor and radial force windings		0.14H/m
Resistance (motor winding)		0.14Ω(an unit)
	(radial force winding)	0.21Ω(an unit)
Equivalent current of permanent magnets		38.0A
Rotor shaft weight(bearingless motor part)		10kg

are measured by the power meters, and the rotational torque is detected by the torque meter. The shaft is supported by the mechanical bearings in the torque meter and the dc generator. The specification of the prototype machine is shown in TABLE 1.

Shaft Suspension And Load Test Results

FIGURES 4(a) and (b) show the waveforms of the rotor radial displacements α_1, β_1, α_2, β_2, U-phase line current i_{um} in the motor winding and U-phase line currents i_{ur1}, i_{ur2} in the radial force windings at the rotational speed rating of 11,000r/min under the rotational torque load rating of 3.6Nm. It is seen that the rotor radial fluctuation is almost 60μm at the unit 1, and it is 30μm at the unit 2. The rotor fluctuations are much smaller than the airgap length of 1.5mm. Therefore, it is confirmed that the rotor shaft is successfully suspended by the electromagnetic forces even in the high speed operation of 11,000r/min. The rotor fluctuations are synchronized with the rotor rotational frequency, therefore, it is caused by the shaft mechanical unbalance. The rotor fluctuation at the unit 2 is smaller than that at the unit 1. Because, the shaft in the unit 2 is connected

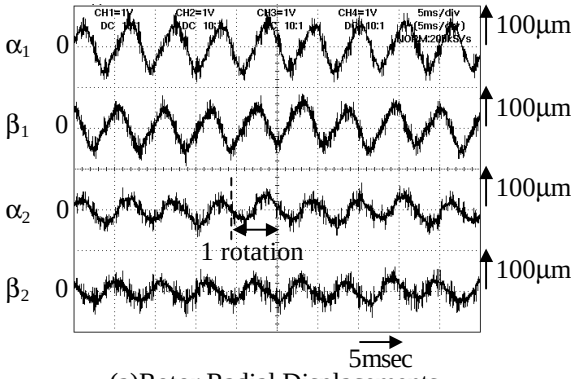

(a)Rotor Radial Displacements

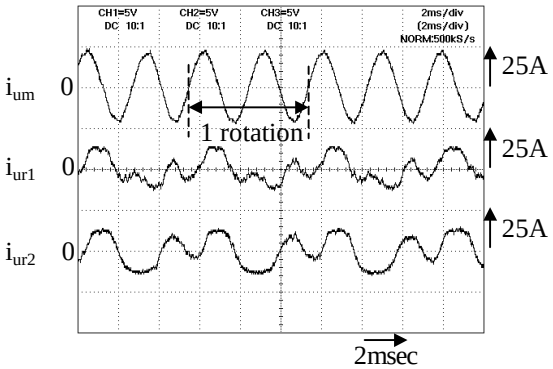

(b)U-phase Line Currents in Motor and Radial Force Windings

FIGURE 4: Waveforms of Rotor Radial Displacements α_1, β_1, α_2, β_2, U-phase Line Current i_{um} in Motor Winding and U-phase Line Currents i_{ur1}, i_{ur2} in Radial Force Windings at Units 1 and 2(11,000r/min, 3.6Nm)

to the torque meter with the mechanical bearings. It is seen in FIGURE 4(b) that the radial force winding currents are synchronized with the rotor rotational frequency, and the same frequency component as the motor winding current slightly exists.

FIGURES 5(a)-(f) show the measurement results of the motor characteristics and the necessary power for the rotor suspension at the rotational speed rating of 11,000r/min. FIGURE 5(a) shows the relation between

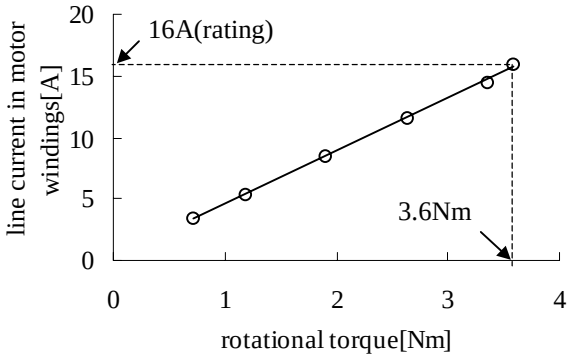

(a)Line Current in Motor Windings and Rotational Torque

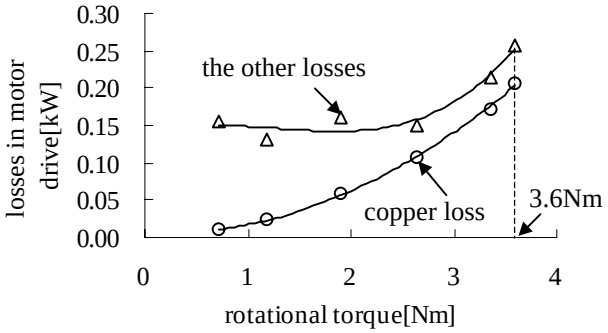

(d)Losses in Motor Drive and Rotational Torque

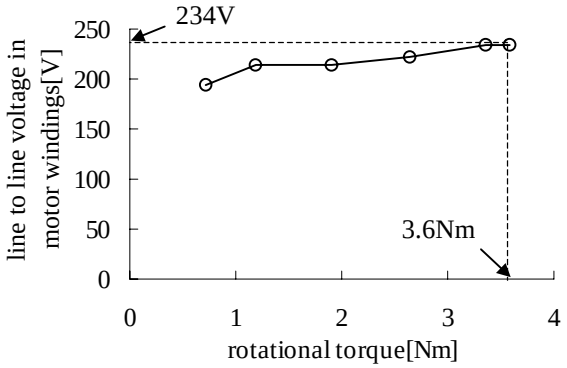

(b)Line to Line Voltage in Motor Windings and Rotational Torque

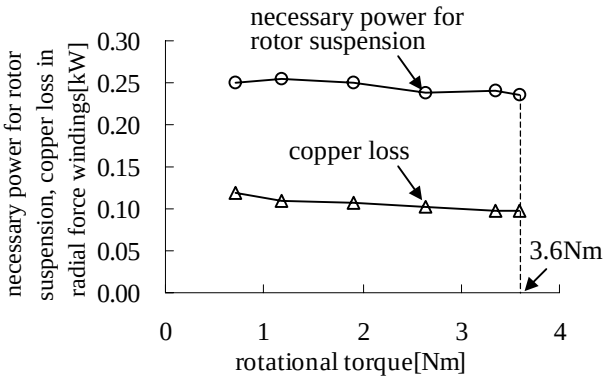

(e)Necessary Power for Rotor Suspension, Copper Loss in Radial Force Windings and Rotational Torque

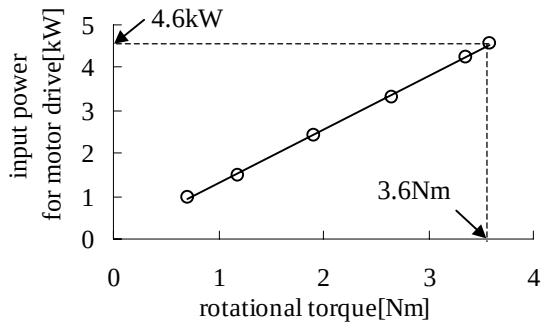

(c)Input Power for Motor Drive and Rotational Torque

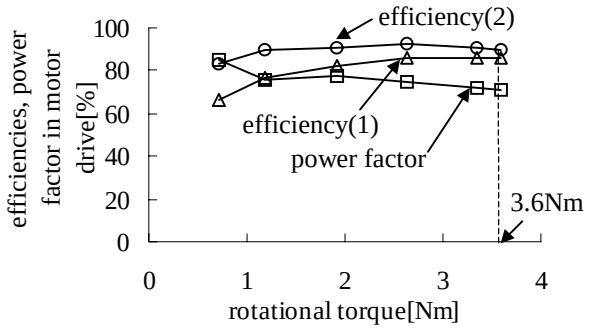

(f)Efficiencies, Power Factor in Motor Drive and Rotational Torque

FIGURE 5: Motor Characteristics and Necessary Power for Rotor Suspension at Rotational Speed Rating of 11,000r/min

the line current in the motor windings and the rotational torque. The line currents in each motor winding are equal in the units 1 and 2, because, the motor windings in the units 1 and 2 are connected in series. It is seen that the line current is linearly increased, then, the line current rating is 16A at the rotational torque of 3.6Nm.

FIGURE 5(b) shows the line to line voltage of the motor windings. The measured values show the sum of the line to line voltages in the units 1 and 2. The line to line voltage is increased in accordance with the increase in the rotational torque, then, it is reached to 234V at the rotational torque rating of 3.6Nm.

FIGURE 5(c) shows the input power for the motor drive. It is seen that the input power for the motor drive is linearly increased, then, it is reached to 4.6kW at the rated rotational torque load.

FIGURE 5(d) shows the losses in the motor drive against the rotational torque variation. The copper loss shows the sum of those in the motor windings of the units 1 and 2. The other losses show the losses in the motor drive except the copper loss, in which the iron loss is included. The copper loss is increased as the

rotational torque is increased, and the other losses are also increased in the rotational torque of more than 2.5Nm. The copper loss and the other losses are almost equal around the rotational torque rating of 3.6Nm.

FIGURE 5(e) shows the necessary power for the rotor suspension and the copper loss in the radial force windings. The necessary power for the rotor suspension and the copper loss show the sums of the measured values in the units 1 and 2, respectively. It is seen that the power for the rotor suspension is slightly decreased. Because, the q-axis flux production results in the increase in the intensity of revolving magnetic field. Therefore, the copper loss is also decreased. The percentage of the copper loss to the necessary power for the rotor suspension was 42% at the rated rotational torque load. The percentage of the power for the rotor suspension to the input power for the motor drive was 5% under the rated torque load, and it was very small.

FIGURE 5(f) shows the efficiencies and the power factor in the motor drive. Two efficiencies denoted by (1) and (2) are shown in FIGURE 5(f). The efficiency(1) shows the percentage of the motor output power to the sum of the input power for the motor drive and the necessary powers for the rotor suspension in the units 1 and 2. The efficiency(2) shows the percentage of the motor output power to the input power for the motor drive, in which the necessary power for the rotor suspension is not included. The maximum value of the efficiency(1) is 86% around the rotational torque load rating of 3.6Nm, however, it is 92% in the efficiency(2).The difference between the efficiencies (1) and (2) is significantly decreased as the rotational torque is increased. Because, it is caused by the decrease in the necessary power for the rotor suspension as shown in FIGURE 5(e). It is seen in FIGURE 5(f) that the power factor is 70% to 80%. It is relatively small to the conventional permanent magnet-type machines. Because, the thickness of the permanent magnets is designed to be equal to the airgap length to generate the radial forces effectively in the prototype machine. Therefore, the synchronous internal voltage is relatively small, resulting in the decrease in the power factor.

CONCLUSION

In the permanent magnet-type bearingless motors, it is necessary that the rotor radial positioning is accurately performed considering armature reaction. In this paper, the rotor radial position control strategy is presented, then, the rotor suspension test and the performance evaluations of the prototype machine as an electric motor are accomplished as follows,

1.The rotor radial position control strategy is presented, in which the information on the airgap flux is obtained by calculating the resultant flux of the field excitation of the permanent magnets and the q-axis flux.
2.The prototype 11,000r/min, 4kW surface-mounted permanent magnet-type bearingless motor was constructed. The rotor shaft was successfully suspended by the proposed control strategy.
3.The necessary power for the rotor suspension as well as the motor characteristics was measured by the load tests. The performance evaluation of the prototype machine is summarized as follows, (1)If the necessary power for the rotor suspension was considered as the loss, the efficiency was 86% at 11,000r/min under the rated rotational torque load. (2)The power factor in the motor drive was relatively small to the conventional permanent magnet-type machines. It is actually expected that the power factor would be made increased by employing a field weakening control in the motor speed controller. As a result, the increase in the efficiency is also expected. (3)The decrease in the necessary power for the rotor suspension would be also expected by balancing the rotor shaft.

REFERENCES

1.T. Ohishi, Y. Okada, S. Miyamoto, Levitation Control of IPM Type Rotating Motor, Proc. of 5th Int. Symp. Magnetic Bearings, pp.327-332, Kanazawa, 1996.
2.S. Silber, W. Amrhein, BEARINGLESS SINGLE-PHASE MOTOR WITH CONCENTRATED FULL PITCH WINDINGS IN EXTERIOR ROTOR DESIGN, Proc. of 6th Int. Symp. on Magnetic Bearings, pp.476-485, Massachusetts, 1998.
3.M. Ooshima, A. Chiba, T. Fukao, M. A. Rahman, Design and Analysis of Permanent Magnet-Type Bearingless Motors, IEEE Trans. IE, vol.43, No.2, pp.292-299, 1996.
4.J. Bichsel, The Bearingless Electrical Machine, in NASA-CP-3152-PT-2, pp.561-573, 1992.
5.R. Schob, N. Barletta, Principle and Application of a Bearingless Slice Motor, Proc. of 5th Int. Symp. Magnetic Bearings, pp.313-318, Kanazawa, 1996.
6.A. Chiba, K. Yoshida, T. Fukao, Transient response of revolving magnet field in induction type bearingless motors with secondary resistance variations, Proc. of 6th Int. Symp. on Magnetic Bearings, pp.461-475, Massachusetts, 1998.
7.O. Ichikawa, C. Michioka, A. Chiba, T. Fukao, An Analysis of Radial Forces and a Rotor Position Control Method of Reluctance Type Bearingless Motors, IEEJ Trans., vol.117, no.9, pp.1123-1131, 1997(written in Japanese).
8.O. Ichikawa, A. Chiba, T. Fukao, Principles and Structures of Homopolar Type Bearingless Motors, Proc. of IPEC-Tokyo 2000, vol.1, pp.401-406, 2000.